Resolution Enhancement of Scanning Tomographic Acoustic Microscope System

Daesik Ko*

ABSTRACT

We proposed to use shear waves instead of longitudinal waves in a STAM (scanning tomographic acoustic microscope system) in which the specimens are solid. For any specimen with a shear modulus, mode conversion will take place at the water-solid interface. Some of the energy of the insonifying longitudinal waves in the water will convert to shear wave energy within the specimen. The shear wave energy is detectable and can be used for tomographic reconstruction.

The resolution limitation of STAM depends on the available angular view and the acoustic wavelength. While wave transmission in most solid specimens is limited to about 20^0 for longitudinal waves, we show that it is about twice that high for shear waves. Since the wavelength of the shear wave is shorter than that of the longitudinal wave, we are able to achieve the high resolution.

In order to compare the operation of a shear-wave STAM with that of the conventional longitudinal-wave STAM we have simulated tomographic reconstruction for each. Our simulation results with aluminum specimen and back-and-forth propagation algorithm showed the resolution of a shear-wave STAM is better than that of a longitudinal-wave STAM.

Ⅰ. Introduction

The STAM (scanning tomographic acoustic microscope) has been proposed as a method to overcome the limitations of the SLAM (scanning laser acoustic microscope). The SLAM operates in the transmission-mode and is designed for high resolution, real time imaging of thin specimens close to the coverslip. At an operating frequency of 100 MHz the SLAM has a lateral resolution of 25 microns. However, the SLAM produces only shadowgraphs and therefore has no axial resolution. To achieve tomograms, the STAM uses several projections and the BFP (back-and-forth propagation) algorithm. The BFP is an efficient method for tomographic reconstruction when the layers of interest in the specimen are planar [1, 2, 3].

As the acoustic wave travels from the water bath of the STAM into the solid specimen there will be mode conversion from longitudinal to shear waves. This phenomenon is a function of the propagation direction of the insonifying acoustic waves in the STAM and has an important bearing on the quality of the tomograms that can be reconstructed.

Three modes of acoustic wave propagation exist in a solid specimen: longitudinal, shear (transverse), and surface acoustic wave. Typically, the wavelengths of both shear and surface waves are shorter than those of longitudinal waves [4]. Therefore, we can expect the use of shear waves in STAM to provide higher resolution.

As the incident angle of the insonifying acoustic wave is increased, the power in the mode-converted shear wave is increased. For normal incidence the displacement of the shear wave is almost parallel to the surface of the specimen, and it is difficult to detect by a knife-edge detector. However a conventional STAM uses oblique incidence and the shear waves can be detected. In all the STAM work previously reported in the literature, only longitudinal waves were used and the primary emphasis was on detection of these waves [5].

To compare the effectiveness of a shear-wave STAM with that of a conventional STAM, we have analyzed the reflection and transmission of acoustic waves as a function of incident angle at the water-solid interface. We have determined the suitable projection angles for several different materials. Finally, we have simulated tomographic reconstructions using the BFP algorithm to investigate the

*Department of Electonic Engineering, Mokwon University

Manuscript Received: March 14, 1996.

effectiveness of the use of shear waves and compared the quality of images produced by a shear-wave STAM with that of a longitudinal-wave STAM.

Ⅱ. Tomographic reconstruction of the STAM system

The STAM system is illustrated in Fig. 1. A number of projections can be obtained by rotating the acoustic transducer or the specimen [1, 2].

As shown in the figure, the acoustic plane waves insonify a planar structure described by the transmission function $t(x, y, z)$. The incident wave is modulated by the object function, and the resulting wavefield produces a dynamic ripple at z_r. A laser beam scans over the surface of the coverslip and is reflected to a knife-edge photo detector which converts the angular modulation of the light beam into an electrical signal related to the wavefield distribution over the coverslip [6].

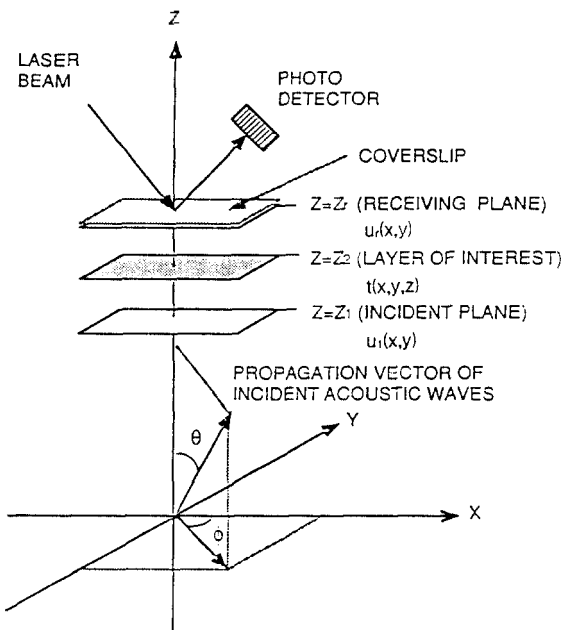

Fig. 1. Schematic diagram of STAM system

The assumed object is homogeneous except for an infinitely thin layer at z_2 that contains elements of different elastic composition. The wavefield at z_1 is $u_1(x, y)$. The wave travels through the object and the wavefield just below plane z_2 is $u_2(x, y)$. The relation between $u_1(x, y)$ and $u_2(x, y)$ can be expressed, using Rayleigh-Sommerfeld diffraction formula, as [6, 7].

$$u_2(x, y) = u_1(x, y) * w(x, y, z_1, z_2) \tag{1}$$

$$\text{with } w(x, y, z_1, z_2) = \frac{|z_2 - z_1|}{2\pi} \frac{1 - jkr}{r^3} e^{jkr} \tag{2}$$

where $r = [x^2 + y^2 + (z_2 - z_1)^2]^{1/2}$, $k = \frac{2\pi}{\lambda}$, λ is the wavelength, and * denotes convolution. In the Fourier domain, Eqs. (1) and (2) become

$$U_2(f_x, f_y) = U_1(f_x, f_y)\, W(f_x, f_y, z_1, z_2) \tag{3}$$

$$\text{with } W(f_x, f_y, z_1, z_2) = \exp\{jk(z_2 - z_1)[1 - f_x^2\lambda^2 - f_y^2\lambda^2]^{1/2}\} \tag{4}$$

where $U_1(f_x, f_y)$ and $U_2(f_x, f_y)$ are the Fourier transforms of $u_1(x, y)$ and $u_2(x, y)$, respectively. The values of the wavefield are sampled at N points in a rectangular grid. Taking these values in a certain order, we can rewrite Eq. (1) as

$$\overline{u_2} = \overline{u_1}\, W(z_1, z_2) \tag{5}$$

For the two dimensional case where there is no variation in the y direction, $\overline{u_1}$ and $\overline{u_2}$ are $1 \times N$ row vectors of sampled values of the wavefields u_1 and u_2, respectively. $W(z_1, z_2)$ is an $N \times N$ Toeplitz matrix, representing forward propagation from z_1 to z_2.

At plane z_2, $u_2(x, y)$ is modified by the transmittance associated with the layer. The wavefield transmitted through the plane z_2 can be written as [7]

$$\overline{u_2'} = \overline{u_2}\, T \tag{6}$$

where $\overline{u_2'}$ is the row vector of the sampled values of the wavefield u_2' and T is the transmittance marix at $z = z_2$ which characterizes the relation between the incident and the transmitted wavefields. If the transmittance is angle-independent, T is a diagonal matrix. If the transmittance is spatial-invariant, T is a Toeplitz matrix. The modified wavefield u_2' propagates to the receiver plane at $z = z_r$ and becomes u_r.

$$\overline{u_r} = \overline{u_2'}\, W(z_2, z_r) \tag{7}$$

where $\overline{u_r}$ is the row vector of the sampled values of the wavefield u_r and $W(z_2, z_r)$ is the forward propagation matrix from z_2 to z_r. The wavefield detected at the receiver plane will be different from u_r because of noise and scattering from other layers. We can back propagate the received wavefield v_r to z_0.

$$\bar{v}_2 = \bar{v}_r W^{-1}(z_2, z_r) \tag{8}$$

where $\bar{v}_2$ and $\bar{v}_r$ are row vectors of the sampled values of the wavefields v_2 and v_r and $W^{-1}(z_2, z_r)$ is the back propagation matrix between z_2 and z_r. Because of noise, the wavefield will not be the same as $u_2(x, y)$. It can be written as

$$\bar{v}_2 = \bar{u}_2 + \bar{n} = \bar{u}_2 T + n \tag{9}$$

whre $\bar{n}$ is a $1 \times N$ row vector representing the noise introduced by the system.

Now, consider M projections generated by plane waves coming in from M different incident angles to insonify the object. From these projections we will obtain a set of equations

$$\bar{v}_{2,m} = \bar{u}_{2,m} T + \bar{n}_m, \quad m = 1, 2, \ldots M \tag{10}$$

The row vectors in Eq. (10) can be combined to form a matrix equation as follows:

$$V = UT + N \tag{11}$$

where V, U, and N are $M \times N$ matrices consisting of M row vectors.

It is assumed that the noise-like undesired signal components, $\bar{n}$, which form the matrix N, will have little correlation from projection to projection. Then an estimate of each element of the transmittance T can be made and is given by [1]

$$t_k^e = \frac{\sum_{m=1}^{M} u_{k,m}^{*T} v_{k,m}}{\sum_{m=1}^{M} u_{k,m}^{*T} u_{k,m}} \quad k = 1, 2, \ldots, N \tag{12}$$

where u_k and v_k are $M \times 1$ column matrices, and * denotes conjugation, the summation is carried out over all the different angles of incidence of the plane wave.

Therefore, if the insonifying angles are greater than the critical angle for longitudinal waves at the interface of the water-specimen, we have to replace the longitudinal waves with shear waves in Eq. (1).

Ⅲ. STAM system using shear waves

At normal incidence, reflection and refraction phenomena are relatively simple since there is no mode conversion between longitudinal and shear waves. However, cases of oblique incidence are more complicated because of refraction. At oblique incidence, mode conversion of the insonifying acoustic waves take place at the interface of water-solid, as shown in Fig. 2 [4].

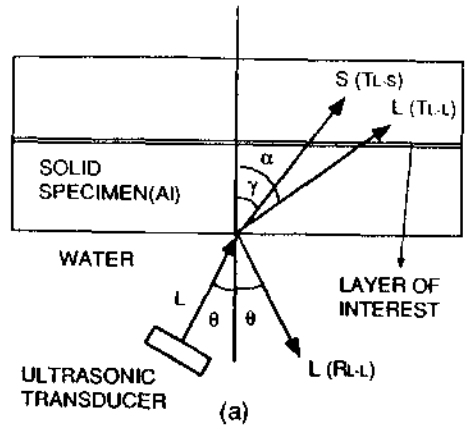

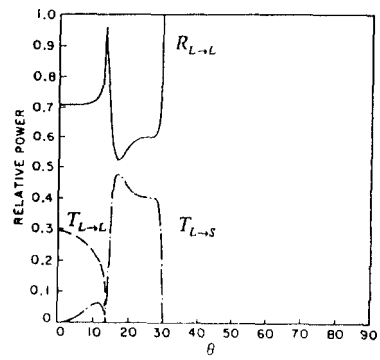

Fig. 2. Reflected and transmitted waves at the interface between water and solid(Al). (a) Mode conversion (b) Reflection and transmission coefficients as a function of incident angle (L: longitudinal, S: shear wave, R: reflection, T: transmission coefficient).

Since both the shear and longitudinal wave velocities in most solids are larger than the longitudinal wave velocity in water, there are two critical angles for each transmitted wave. The critical angle for longitudinal and shear waves is obtained by substituting for the angle of refraction in Snell's law.

The transmission and reflection of the acoustic waves at an interface between two media can be obtained by Eqs. (13), (14) and (15) [8, 9].

$R_{L\to L} =$

$$\frac{\cos\alpha - a\gamma\cos\theta[1-2\sin\gamma\sin 2\gamma(\cos\gamma-(1/b)\cos\alpha)]}{\cos\alpha + a\gamma\cos\theta[1-2\sin\gamma\sin 2\gamma(\cos\gamma-(1/b)\cos\alpha)]} \quad (13)$$

$$T_{L\to L}=$$

$$\frac{2\cos\theta\cos 2\gamma}{\cos\alpha + a\gamma\cos\theta[1-2\sin\gamma\sin 2\gamma(\cos r-(1/b)\cos\alpha)]} \quad (14)$$

$$T_{L\to S}=$$

$$\frac{(2a/b)\sin 2\theta\cos\alpha}{\cos\alpha + a\gamma\cos\theta[1-2\sin\gamma\sin 2\gamma(\cos\gamma-(1/b)\cos\alpha)]} \quad (15)$$

Where $R_{L\to L}$, $T_{L\to L}$ and $T_{L\to S}$ are reflection coefficient of the longitudinal wave, transmission coefficient of the longitudinal wave and transmission coefficient of the shear wave for an incident longitudinal wave, respectively. $a=\frac{V_2}{V_L}$, $b=\frac{V_L}{V_S}$, V_2 is velocity in water, V_L and V_S are longitudinal and shear-wave velocity in solid, ρ_1 is the solid density, ρ_2 is the water density and θ, α, γ are shown in Fig. 2-(a). As an example, if an acoustical wave s are transmitted into aluminum from an incident longitudinal wave in water, the transmission and reflection coefficients as a function of the incident angle is obtained as shown by Fig. 2-(b) [4]. In Fig. 2-(b), as the angle of the incidence increases, the transmission of the shear wave increases and the transmission of the longitudinal wave decreases becoming zero at the critical angle. If the incident wave in water reaches an angle greater than longitudinal critical angle, there is no longer a refracted longitudinal wave in aluminum but only a shear wave. At an angle of incidence of approximately 17^0, almost half the incident power is converted to power in the shear wave; if the angle of incidence is greater than the shear wave critical angle, the water-aluminum interface is a perfect reflector.

In order to determine the usable range of incident angle for projections, we computed critical angles for longitudinal and shear waves. Table 1 shows the critical angles of several solids and we can use this data in designing a STAM system.

In Table 1, it is seen that the typical critical angle of the longitudinal wave is limited to 20°and that of the shear wave to about 40°. Since shear waves can not propagate in fluids and some solids such as rubber and vinyl, our system is restricted to specimens that can support shear waves.

The theoretical resolution limitation of STAM depends on the available angular view and the acoustic wavelength [1]. By using shear waves, we can increase the angular range. Since the wavelength of shear wave is shorter than that of longitudinal wave, we are able to achieve the high resolution with shear-wave STAM.

We simulated STAM tomographic reconstructions with this conditions. That is, when we used the BFP algorithm with an aluminum specimen, we used longitudinal waves in the range between 0°and the longitudinal critical angle of ±13°and shear waves between ±13°and shear critical angle of ±29°.

Table 1. Acoustical characteristics of the materials [4]

Material	L-wave Velocity (m/s)	S-wave Velocity (m/s)	L-wave critical angle	S-wave critical angle
Aluminum	6420	3040	13.5	29.5
Brass	4700	2100	18.6	45.5
Copper	5010	2270	17.4	41.3
Fused quartz	5960	3760	14.5	23.5
Pyrex glass	5640	3280	15.4	27.2
Steel	5900	3200	14.7	27.9
Molibdenum	6300	3400	13.7	26.1
Nickel	5600	3000	15.5	30.0
Si nitride ceramic	11000	6250	7.8	13.8
Vinyl	2230		42.2	

Ⅳ. Experimented simulation results

In order to investigate the performance of our technique, we use in our simulated experiment a planar structure as the specimen. It is assumed to be attenuation free except for two thin layers separated by a distance of four wavelengths. The attenuation pattern of the layers are designed to show the resolution and is shown in Fig. 3.

Top layer has a binary attenuation pattern with regions of greatest opacity being 50% transparent and others, 100% transparent to the acoustic waves. For our simulations we assumed perfect detection, that is that we could detect the shear wave, compensate for the effects of the antisymetric knife-edge transfer function [1].

We simulated nine projections with transducer rotation scheme and reconstructed the images with BFP. The results are shown in Fig. 4. Fig. 4-(a) shows images obtained using longitudinal waves with projection angles from -48° to +48°. Fig. 4-(b) shows images obtained using shear waves with projection angles from -58° to -26° and from +26° to +58° with transducer rotation.

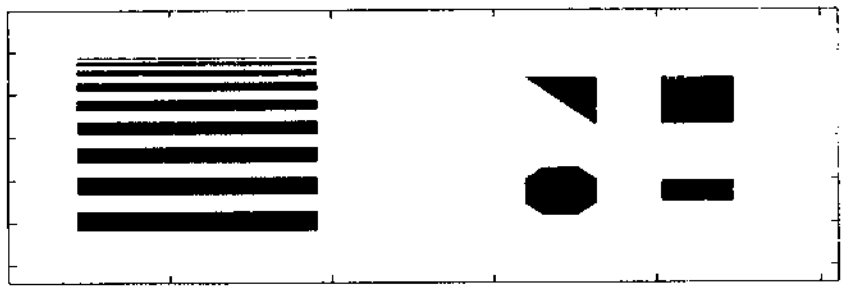

Fig. 3. Attenuation patterns for simulations

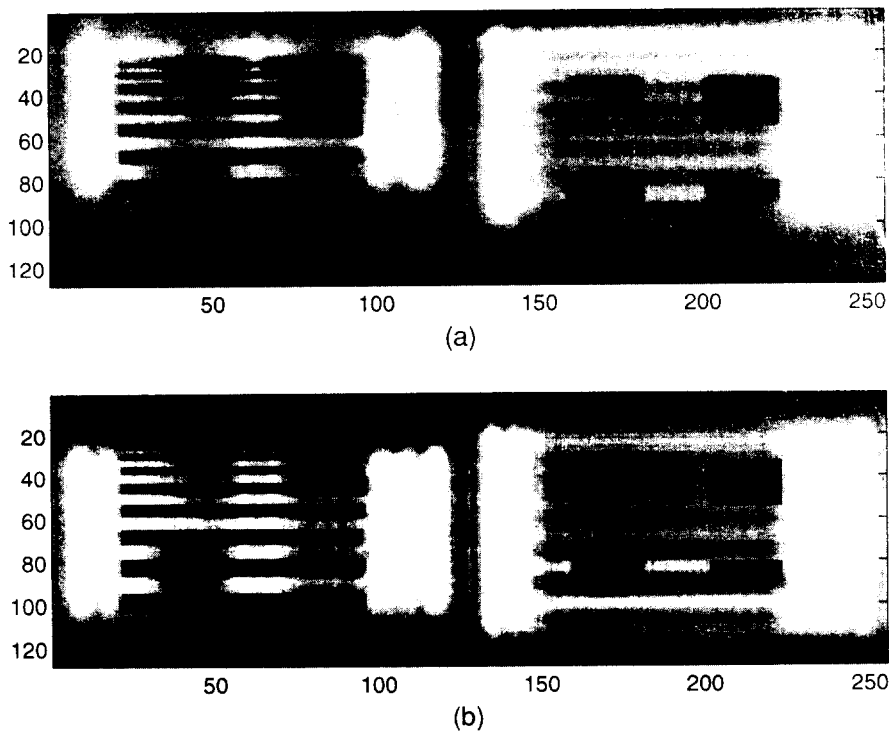

Fig. 4. Simulated images obtained from 9 projections with transducer rotation. (a) longitudinal-wave images (b) shear-wave images (layer separation is four wavelengths).

As shown in Fig. 4, the contrast and resolution of the shear-wave image are better than those of the longitudinal-wave image. In order to analyze influence of the shear wave in the specimen rotation, we simulated the reconstruction by a similar technique. The specimen was assumed to be rotated circularly with a constant angular increment of 40°through 360°to produce nine projections.

The results are shown in Fig. 5. Fig. 5-(a) shows images obtained with longitudinal waves, the angle of incidence of acoustic wave $\theta = -10°$. Fig. 5-(b) shows images obtained with shear waves, the angle of incidence of acoustic wave $\theta = -21°$.

Fig. 5 shows that the tomographic image made with shear waves has better image quality.

V. Conclusions

In this paper, we proposed a technique for resolution enhancement of the STAM system. We reviewed the BFP algorithm for reconstructing tomograms of microscopic objects and investigated the mode conversion of insonifying acoustic waves in STAM system. We showed that wave transmission of longitudinal waves in most solid specimens is limited to about 20^0 but wave transmission of shear waves is about 40^0.

In order to compare the performance of a shear-wave STAM with that of the conventional longitudinal-wave STAM we simulated tomographic reconstructions with layer separation of four wavelengths. In transducer rotation and specimen rotation scanning, our simulation results showed that the resolution of a shear-wave STAM is better than that of a longitudinal-wave STAM.

References

1. Z. C. Lin, H. Lee and G. Wade, "Scanning Tomographic Acoustic Microscope-A Review," *IEEE Trans. Sonics Ultrason.*, vol. SU-32, pp. 168-180, 1985
2. R. Y. Chiao, H. Lee, "Recent Advances in Scanning Tomographic Acoustic Microscopy," *International Journal of Imaging Systems and Technology*, pp. 334-353, 1991
3. S. Meyyappan and G. Wade, "An Iterative Algorithm for Scanning Tomographic Acoustic Microscopy", Ultrasonic Imaging, Vol. 13, pp. 334-346, 1991
4. G. S. Kino, *Acoustic Waves*, Prentice-Hall, Chapter 2,

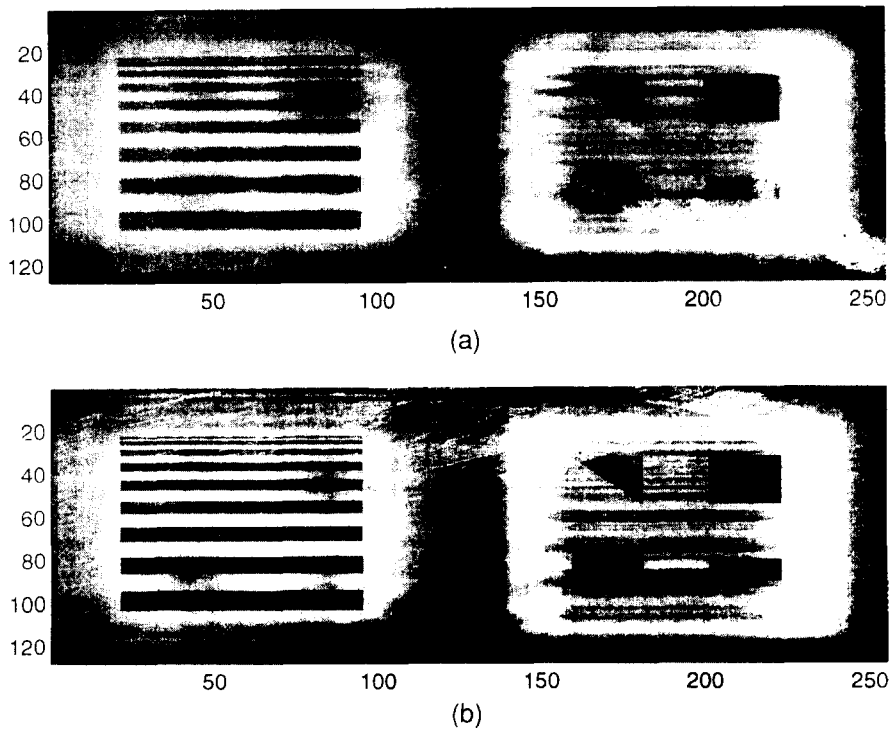

Fig. 5. Simulated images obtained from nine projection with specimen rotation. (a) longitudinal-wave images, (b) shear-wave images(layer separation is four wavelengths).

1987

5. D. S. Ko, A. Meyyappan and G. Wade, "A Planar Ultrasonic Tomography using Shear Waves," *IEEE southwest symposium*, 1996
6. S. D. Kent, H. Lee, "Quantization Bit Rate Reduction in Scanning Tomographic Acoustic Microscopy," *IEEE Trans. Ultrason. Feroelectrics, and Frequency Control*, Vol. 42, pp. 464-477, 1995
7. J. W. Goodman, *Introduction to Fourier Optics*, McGraw-Hill, New York, 1968, chapter 3
8. B. Noorbehesthi, "Spatial Frequency Characteristics of Opto-Acoustic Transducer," Ph. D. Dissertation, University of California, Santa Barbara, 1980
9. T. Plalucha and P. Cawley, "An Investigation of the Accuracy of Oblique Incidence Ultrasonic Reflection Coefficient Measurements," *J. Acoust. Soc. Am.*, Vol. 96(3), pp. 1651-1660, 1994

▲Dae Sik Ko

Dae Sik Ko received the B.S., M.S. and Ph.D degree in eletronic engineering from Kyunghee University, Seoul, Korea, in 1982, 1987 and 1991, respectively.

From 1995 to 1996, he joined Dept. of Electrical and Computer Engineering of the University of California, Sanata Barbara(UCSB) as a Post-Doctoral researcher, where he worked on Acoustic Microscopy(SLAM, STAM).

He is currently working with Dept. of Eletronic Engineering of Mokwon University as an Associate Professor. He is currently a member of the IEEE and Editor of the Acoustical Society of Korea, and his research interests are acoustic microscopy, nondestructive testing, and signal processing.